Role of the amazon outflow on the barotropic tide on the amazonian shelf

Fabien Durand, Laurent Testut, Julien Jouanno, Alice César Fassoni-Andrade

Role of the Amazon outflow on the barotropic tide on the Amazonian shelf

Fabien Durand*[1,2], Laurent Testut[3], Julien Jouanno[1], Alice César Fassoni-Andrade[1,2]

[1]LEGOS UMR5566, CNRS/CNES/IRD/UPS, 31400 Toulouse, France
[2]Laboratório de Geoquímica, Instituto de Geociencias, Universidade de Brasilia, Brasilia 70.910-900, Brazil
[3]LIENSs UMR 7266, CNRS- La Rochelle University, 17000 La Rochelle, France
*corresponding author: fabien.durand@ird.fr

Highlights

- A numerical study of the impact of the Amazon discharge on the magnitude of the tide at its mouth
- The discharge induces a rise of tidal amplitude of ten centimeters at the coast
- This rise is associated to a rise of mean sea level also of ten centimeters
- This tidal amplification is partly attributable to the rise of mean sea level
- It is also partly attributable to the vertical density stratification of the Amazon plume
- Profound impacts of future sea level rise can be expected on tidal flooding and on socio-economic dynamics of the Amazon delta

Abstract

The Amazon yields the largest freshwater discharge to the world ocean, outflowing on a shallow, macro-tidal shelf. Its plume dynamics is complex and the impact of the discharge on the tidal properties on the adjoining shelf remains poorly understood. Through a series of numerical modelling experiment, we investigate the interaction between the Amazon discharge and the tide over the Amazonian shelf. We find that the runoff is responsible for a rise of the M2 tidal amplitude of ten cm in the embayment between Cabo Norte and Cabo Cassipore. The runoff also induces a rise of the mean sea level there, of ten cm as well. Such a one-to-one sensitivity of the tidal amplitude and of the mean sea level over this region is quite unique among the world coastline. The modulation of the bottom friction by the thickness of the water column as well as by the vertical density stratification in the Amazon plume appears to be the main forcing factor of this response. Our numerical sensitivity experiments suggest that the seasonal variability of the Amazon discharge has little impact on the temporal variability of the tidal characteristics over the Amazonian shelf.

1. Introduction

The Amazon, draining most of the northern part of South America, yields the largest river discharge on Earth. It outflows on a broad, shallow shelf (Fig. 1), characterized by a macrotidal regime (Beardsley et al., 1995). Its discharge shows marked seasonal variations, lowest in December (100'000 - 150'000 m^3/s), and highest in May (300'000 m^3/s) (Fig. 2). Several factors make the Amazon outflow unique. Because of its magnitude, the classical estuarine salinity frontal structure is pushed far offshore, out of the estuary, in the open ocean (Fontes et al., 2008). The location of the outflow right at the equator makes the plume dynamics peculiar. The freshwater plume dispersal is governed by an intricate physics, involving the large-scale North Brazil Current, the local wind, and the tidal currents (Nikiema et al., 2007; Fontes et al., 2008; Molinas et al., 2014; Ruault et al., 2020). The Amazon freshwater outflow is known to impact both the local and the remote mean sea level, through the combination of its mass and halosteric effects (Giffard et al., 2019; Durand et al., 2019). On account of the strength of the tide and of the shallow depth of the near-shore Amazonian shelf (Fig. 1), the tide is prone to generate strong shallow-water overtides and compound tides there (Gallo and Vinzon, 2005). Being bordered by a sharp continental slope, with strong vertical stratification of the water column in all seasons, the barotropic tide was found to be instrumental in the sedimentary faciology of the Amazon shelf, through the internal tide it radiates (Molinas et al., 2020).

Over the Amazonian shelf, the impact of the ocean tide on the spatial structure of the Amazon plume has been well established (Molinas et al., 2014; Ruault et al., 2020). On the other hand, the tide is known to be significantly impacted by the river flow in various estuarine systems worldwide (see e.g. Haigh et al 2019 for a review of the past studies). In the Amazon, the tide was shown to vary seasonally inside the estuary, as a response to the seasonal variability of the river discharge (Gallo and Vinzon, 2005; Kosuth et al., 2009). However, up to date little is known about the role of the Amazon outflow on the characteristics of the tide on the adjoining oceanic shelf. There are various processes through which discharge can influence the tide in large, shallow deltaic systems or semi-enclosed basins. First, by modulating the mean sea level, the river discharge can linearly modulate the vertical dilution/concentration of the tidal

energy flux, via the so-called shoaling effect (Haigh et al., 2019). This effect competes with the barotropic modulation of the bottom friction, which tends to induce higher tidal amplitude in conditions when the mean sea level is higher (see Talke and Jay, 2020, for a review). Baroclinic modulation of the bottom friction can also be a prominent factor: the freshwater discharge can induce a vertical stability of the water column at subsurface, which in turn is less prone to turbulent mixing and momentum dissipation at the bottom of the ocean (Kang et al., 2002; Muller et al., 2014). The specific geology of large river outflows can also impact the tide. Wide parts of the Amazonian shelf are consistently covered by fluid mud banks deposited by the river plume (Nittrouer et al., 2021). Gabioux et al. (2005) and Fontes et al. (2008) analyzed the impact of these specific sedimentary features on the bottom friction. They concluded that the fluid mud induces a weak momentum dissipation of the barotropic tide, hereby favouring large tidal amplitude at the coast.

The strength of the freshwater discharge, the magnitude of the tide and the broad, shallow shelf altogether make this region a relevant case-study of the impact of the river discharge on the coastal tide off the delta mouths. The current period of history tends to be considered as the last epoch when the Amazon hydrodynamics remains primarily unaffected by anthropogenic influences (Latrubesse et al., 2017; Nittrouer et al., 2021). It is important to understand the water level variability at the mouth of the Amazon over a broad range of timescales, in the 21st century context of ongoing sea level rise (Church and White, 2011) and of profound changes in the hydrology of the Amazon watershed (Latrubesse et al., 2017), where several large coastal cities of the Amazon delta are already massively exposed to coastal flooding (Mansur et al., 2016; Szabo et al., 2016). Hence it appears timely to decipher the interactions between the Amazon outflow and the tide.

The aim of the present study is to assess the impact of the Amazon outflow on the tidal characteristics on the Amazonian shelf, through a set of dedicated ocean numerical modeling experiments. Section 2 presents our modelling approach and the various datasets we utilized. In Section 3, we present the model validation. Our results are shown in Section 4, followed by a discussion in Section 5 and concluding remarks in Section 6. Note that our focus is not on the Amazon mouth but rather on the continental shelf situated to the North of it, as our model domain does not extend within the Amazon delta per se.

2. Data and methods

2.1 Model

We use a regional configuration of the NEMO 3.6 ocean general circulation model (Madec et al., 2014). It consists of a 3-level, two-way nested set of grids, with varying resolution from 1/4° (over the whole tropical Atlantic) to 1/12° (over the western tropical Atlantic) and 1/36° (over the Amazonian shelf and slope region). The three embedded domains are displayed in Figure 1. The model is strictly identical to the one used by Ruault et al. (2020), and largely derived from the one used in Hernandez et al. (2016), Giffard et al. (2020) and Gévaudan et al. (2021). We refer to these past papers for extensive validation of the model. For the sake of conciseness in the present paper we will focus mostly on the tidal validation. The model has a vertical grid of 75 levels, identical across the three subdomains, with 12 levels in the upper 20 m. The three domains are coupled online through AGRIF library (Blayo and Debreu, 1999; Debreu et al., 2008). The motivation for this nesting strategy is to allow simultaneously the resolution of the fine spatial scales that are expected to be instrumental for capturing the hydrodynamics of the Amazonian shelf, as well as the basin-scale three-dimensional thermohaline dynamics, which is known to be important in the vertical stratification of the western equatorial Atlantic (e.g. Hernandez et al., 2016). The AGRIF algorithm allows a seamless, numerically consistent exchange of information among the various sub-domains (Blayo and Debreu, 1999; Debreu et al., 2008). The coarse resolution of the outer domain ensures a tractable numerical cost overall. The vertical turbulence closure uses a generic-length-scale scheme (Umlauf and Burchard 2003) with k-epsilon formulation (see Reffray et al. 2015 for a description of its implementation in NEMO). In the bottom boundary layer the friction is quadratic, with a drag coefficient of 10^{-3}. The free-surface formulation follows a time-splitting scheme, solving separately the fast barotropic transients (among which is the tide) and the lower frequencies. The bathymetry was taken from GEBCO atlas (Weatherall et al., 2015). The river discharge of the Amazon system (comprising the contributions of the Amazon itself, as well as Tapajos and Xingu rivers) and Para/Tocantins system are injected in the model as mass sources with zero salinity, through the open boundaries located at the estuaries mouths.

We use the discharge estimates provided by HYBAM (2018) hydrological observatory. The atmospheric forcing (wind, heat and freshwater fluxes) is taken form DFS5.2 product (Dussin et al., 2016). The model tide is forced by the astronomical potential of all major high frequency tidal constituents (M2, S2, N2, K2, K1, O1, Q1, and P1), and the same constituents are applied at the boundaries of the outer domain, from FES 2012 tidal atlas (Carrère et al., 2012). The period of simulation is 2005-2015 and only the period 2014-2015 is considered in the present study. We performed various sensitivity experiments to decipher the mechanism of discharge-tide interaction, by switching on and off the discharge forcing and/or the ocean vertical density stratification. The set of model experiments we performed is summarized in Table 1.

2.2 Observations

To validate the large-scale patterns of the tide, we relied on FES2014 tidal atlas (Carrère et al., 2016). As the quality of global tidal atlases in poorly-documented coastal regions such as the mouths of the Amazon is largely unknown, we complemented the tidal atlas with all historical tide-gauge records we could access over the region of interest. They were obtained from the Brazilian Navy (www.marinha.mil.br/chm/estacoes-maregraficas; last accessed 17/5/2021). They amount to five records in total, with a duration limited to one month for most of them (Table 2). The records have a hourly frequency. Their locations are displayed on Figure 1b. Each record was visually inspected and inconsistent values were discarded. Both model outputs (at hourly frequency) and in situ records were subjected to harmonic analysis, through the Tidal Toolbox (Allain, 2016).

3. Model validation

The model performance was successfully assessed for the regional circulation patterns as well as for its thermohaline three-dimensional structure over the western tropical Atlantic in the past studies of Hernandez et al. (2016), Giffard et al. (2020) and Ruault et al. (2020). In the present paper we will thus primarily restrict our validation to our specific features of interest, namely the tidal variability in the Amazonian shelf

region (Sections 3.1 and 3.2). A validation of the vertical stratification in the region off the Amazonian shelf is provided in Section 3.3.

3.1 Large-scale tidal patterns

The tide over the Amazonian shelf is semi-diurnal, dominated by M2 and S2 constituents (Gallo and Vinzon, 2005; LeBars et al., 2010). Figure 3 compares the amplitude of these constituents between our model and FES2014. It is seen that the model successfully captures the two coastal maxima of M2 and S2 amplitude, located to the north-west and to the south-east of the mouths of the Amazon. Beardsley et al. (1995) identified the north-western region, between the two capes Cabo Norte and Cabo Cassipore, as an embayment which cross-shore length is close to the resonant length for semi-diurnal tidal constituents. In addition, they suggested that the bending of the coastline around Cabo Norte precludes leakage of tidal energy from this region towards the mouth of the Amazon, hereby favouring maximal tidal range there. For both M2 and S2, the model shows an under-estimation of the amplitude in the core of this north-western maximum (2°N, 50.5°W), typically by 30 cm and 10 cm respectively. In contrast, the model shows an over-estimation of both M2 and S2 amplitudes along the south-eastern coastal maximum (1°S-2°S, 44°W-48°W), by 30 cm and 20 cm respectively. We remind that our model was not especially calibrated for the tide, in the sense that we did not carry out any regional tuning of the bottom roughness, nor of the bathymetry, unlike the past numerical modeling studies over the region specifically dedicated to the tidal dynamics (Gallo and Vinzon, 2005; Fontes et al., 2008; LeBars et al., 2010; Molinas et al., 2014). We remind that the objective of this study is not to produce a novel reference tidal atlas of the area, but to study the river outflow – tide interaction. In that perspective, the broad agreement between the model and FES2014 atlas appears satisfactory.

3.2 Tidal validation in the vicinity of the Amazon mouths

In order to quantify the degree of realism of our model at the river mouth we assessed the tide using the five available tide gauges (Fig. 1). Because our regional focus lies in the vicinity of the Amazon mouths, it is necessary to assess specifically the realism

of the modeled tide there. We considered the two dominant tidal constituents, M2 and S2, which altogether capture the majority of the total tidal signal over the region (Beardsley et al., 1995). For each tide gauge station, we computed the error of the model tide as the modulus of the complex difference for these two constituents together, following the method by Andersen et al. (1995), used in numerous past studies (e.g. Krien et al., 2016;):

$$|\Delta z| = \left| A_m e^{i\theta_m} - A_o e^{i\theta_o} \right|$$

The total error at a given station is:

$$\sigma = \sqrt{\frac{1}{2} \sum_{N_{constituents}} |\Delta z|^2}$$

Table 2 shows our results. The modeled tide appears in good agreement with the observed values for the two northernmost tide gauge stations (Ponta do Céu and Ponta Guará), with complex errors of 8 cm and 9 cm respectively. These values are in line with the typical performance of regionally-tuned high-resolution tidal models, such as Molinas et al. (2014). In contrast, the realism of the modeled tide appears significantly worse when we get closer to the Amazon mouths, with errors of order 40 cm and above, that is about twice worse than Molinas et al. (2014). This can be explained by the poor numerical formulation of the open boundary of the Amazon outflow (where no radiative condition could be implemented, which could induce spurious reflection of the tidal energy there), by the poor quality of GEBCO bathymetry in this region of narrow channels (Le Bars et al., 2010; Fassoni-Andrade et al., 2021), as well as by the too coarse horizontal resolution of the model grid. As a result, we will refrain from analyzing our model outputs in the immediate vicinity of the mouths of Amazon delta, in the present study. Overall, the good quality of the modeled tide to the North of the equator gives us confidence in the subsequent analysis of the tide-discharge interactions there, as we shall see in Section 4.

3.3 Vertical stratification of temperature and salinity off the Amazon mouth

As we shall see in the following section, the vertical density stratification is an important ingredient of the plume-tide interaction on the Amazon shelf. A thorough validation of the model stratification there is challenging though, on account of the poor coverage of observational atlases there. Figure 4 presents a comparison between the

model temperature and salinity vertical structure and World Ocean Atlas climatology (Locarnini et al 2013, Zweng et al 2013), along the north-south section off the Amazon mouth in its area closest to the shore documented in the atlas (hence starting at 4°N). It is seen that the model successfully captures the upper ocean temperature field, as well as the thermocline structure, with a 20°C isotherm gently sloping upwards from about 150 m in the slope region to about 135 m at 10°N. The model shows a warm bias of about 1°C over the upper 50 m. Such a bias is largely in line with state-of-the-art numerical models of the area (Gévaudan et al., 2021). The structure of the halocline is also decently captured by the model, with a 36 PSU isohaline sloping downwards from about 15 m at 5°N to about 30 m at 10°N. Shoreward of 5°N, the model clearly shows the signature of the Amazon freshwater plume in the upper 10 m, which is not seen in the observations, most probably on account of the very poor observational coverage there. However we investigated the vertical structure of the model salinity in the shelf region within the salt wedge by comparing with the handful of hydrographic sections carried out during AMASSEDS program (Lentz and Limeburner, 1995) and we could concluded to a good consistency of the model and the *in situ* profiles (see Ruault et al., 2020).

4. Results

4.1 Mean picture

The model mean tidal range is displayed in Figure 5a. It was computed as the long-term mean of the difference between maximum water level and minimum water level, considered over a 24 hour-long moving window centered on every time step of the model outputs. In line with the patterns of M2 and S2 amplitude, we find again the two regional maxima lying on either side of the mouths of the Amazon. The maximum range, in excess of 5 m, is seen in the coastal embayment immediately to the North of Cabo Norte (50°W, 2°N). Figure 5b shows the difference in tidal range between the REF simulation and the NoAMZ sensitivity experiment, which results from discarding the Amazon freshwater discharge from the model forcing. It is seen that the Amazon outflow induces a rise of the tidal range of about 14 cm in the region of Cabo Norte, reaching a maximum value of 22 cm at the coast. Over the rest of the domain, the influence of the Amazon outflow is modest, typically less than 6 cm in absolute values. One exception is

the immediate vicinity of the Amazon mouths around (50.5°W, 0.5°N) and around (49°W, 2°S), where we will refrain from attempting any further analysis on account of the doubtful quality of the modeled tide there (see Section 3). At this point, it is interesting to investigate which tidal constituent is responsible for the differences between REF and NOAMZ. Fig. 5c shows the difference of M2 amplitude between REF and NOAMZ. We remind that the tidal amplitude amounts to half of the tidal range, by definition. It is seen that the rise of tidal range induced by the Amazon discharge is primarily due to the increase of M2 amplitude (note that the range of the color bar in Fig. 5b is exactly double that of Fig 5c, for convenience). Hence in the following we will restrict our analyses to M2 tidal constituent. Aside from this rise in tidal range, the Amazon outflow is also responsible for a rise of the mean sea level (Fig. 5d), as intuitively expected from such a mighty discharge. It exceeds 30 cm in the immediate vicinity of the mouths of the Amazon. In the region of Cabo Norte where we observed the maximal difference in tidal amplitude between the two simulations, it amounts to around 12 cm. In other words, when the Amazon outflow is activated in the model, the rise in mean sea level there is of the same order of magnitude as the rise in tidal amplitude. As a result, in this embayment the inclusion of the Amazon outflow induces a twofold rise of the level of the high waters, through the combined effect of the increase of mean sea level and increase of the tidal amplitude.

4.2 Seasonal variability

As the Amazon discharge is variable along the seasonal cycle (Fig. 2), it is interesting to assess the temporal variability of the pattern revealed in Section 4.1. To do so, we performed a moving-window harmonic analysis over the 2 years of the model simulations, considering temporal windows of 32 days, as in Tazkia et al. (2017). This duration of 32 days is known to be long enough to separate the main semi-diurnal tidal constituents dominating the tidal signal over our area (Pugh and Woodworth, 2014). We spatially averaged the tidal amplitude over the "Cabo Norte" box (hereafter noted "CN"), displayed in Figure 5c. Indeed, this box encompasses the area of maximum impact of the Amazon discharge. Figure 6 shows the time evolution of M2 amplitude averaged over CN box for the REF simulation (in blue) and for the NOAMZ ("no Amazon runoff") sensitivity experiment (in red). It is seen that both curves vary in concert, keeping a roughly

299 constant offset of 10-15 cm. This means that the impact of the Amazon outflow on the
300 M2 amplitude is primarily independent of the seasonality of the discharge. However, it is
301 seen that M2 amplitude does show a very distinct seasonal cycle similar in both
302 simulations, with highest amplitude in boreal fall and lowest amplitude in boreal spring
303 in both years we simulated. The peak-to-peak difference of this seasonal variability of
304 M2 amplitude is of order 10-15 cm, which is comparable with the mean impact of the
305 Amazon outflow on M2 amplitude there.

306 Although a detailed analysis of the mechanisms responsible of this seasonal
307 variability of the tide over CN box is out of the scope of the present study, we performed
308 two additional sensitivity experiments to acquire some insights in the underlying
309 dynamics. These experiments are named BRTP (for "barotropic") and BRTPnoAMZ (for
310 "barotropic without Amazon runoff"). In both these experiments, we imposed a uniform
311 density throughout the model domain. This was done by imposing at each model time
312 step a constant, uniform value to the model temperature and salinity 3D fields, of 28°C
313 and 38 units (in the practical salinity scale) respectively. We similarly analyzed the
314 temporal variability of the tide in BRTP and BRTPnoAMZ experiments over CN box
315 (respectively dark green curve and light green curve in Fig. 6). It is seen that both
316 barotropic simulations show a very similar seasonal evolution of M2 amplitude,
317 consistently within 1 cm one from the other. Both barotropic simulations show a M2
318 amplitude consistently between that of REF and that of NoAMZ. It is also interesting to
319 see that their seasonal evolution of M2 amplitude is similar to REF and NOAMZ
320 simulations, with minimum amplitude in spring, maximum amplitude in fall. The peak-
321 to-peak range of seasonal variability amounts to about 8 cm, comparable with (but
322 somewhat smaller than) the two vertically-stratified simulations REF and NOAMZ.

323 To understand the key parameter responsible for the difference of tidal
324 amplitude between REF and NOAMZ, we computed the monthly de-tided sea level over
325 CN box (Fig. 7a). In both simulations, no clear seasonal variability can be seen. Rather,
326 some marked intra-seasonal fluctuations of the sea level appear, with typical magnitude
327 of 5 cm. The offset between the two simulations consistently remains around 10-15 cm,
328 in line with the difference of long-term mean sea level we have seen in Figure 5d. In
329 particular, none of the simulations exhibits a seasonality of the sea level correlated with
330 the evolution of M2 amplitude seen there. However, if we consider an offshore box
331 encompassing the outer continental shelf and slope region (displayed in Figure 5c), both

simulations show a prominent seasonal variability of the de-tided sea level, minimum in boreal spring and maximum in boreal fall, with peak-to-peak amplitude of about 15 cm, and in phase with the evolution of the tidal amplitude in the CN box.

5. Discussion

As we have seen in the previous section, the impact of the Amazon discharge on the tidal characteristics appears maximal at the coast, in the embayment located immediately to the North of Cabo Norte, in the core of maximal tidal range observed over the Amazonian shelf. This impact appears largely independent of the time. There, the Amazon outflow induces a ten cm increase of the mean sea level, as well as a ten cm increase of tidal amplitude. As a result, the level of high tide water shows a twofold increase, viz. twenty cm (not shown), compared to a numerical modeling framework not accounting for the Amazon discharge. This very large sensitivity of the tidal amplitude change in Cabo Norte region with regards to the local sea level change, amounting to a ratio of about 1:1, appears quite unique among the world coastlines, based on the global studies of Pickering et al. (2017) or Schindelegger et al. (2018). Indeed, both these studies concluded to a much smaller sensitivity of the tide to the regional mean sea level in the coastal ocean. Based on a comprehensive, worldwide observational dataset as well as on global modeling of future sea level rise scenarios, they reported typical ratio values of about 1:10 to 1:5, i.e. a rise in tidal amplitude of order one-tenth to one-fifth of the corresponding rise in regional sea level. As said in the introduction, the sensitivity of the tidal amplitude to the sea level in the shallow regions (such as the Amazonian shelf) involves several competing effects (Haigh et al., 2019; Talke and Jay, 2020). The first one is a linear shoaling/deepening effect, yielding increased tidal amplitude when the water depth decreases. It is simply explained by the vertical convergence/divergence of the tidal energy flux radiated shoreward from the deep ocean towards the shallow coastal domain. This effect is not consistent with the tidal amplification seen in REF simulation with regards to NoAMZ. The second effect is frictional: the higher the mean sea level, the lower is the magnitude of the momentum dissipation at the bottom. This effect thus favours increased tidal amplitude when the water depth increases. In the region of Cabo Norte, this frictional effect appears consistent with our model experiments: the increase in mean sea level induced by the Amazon outflow is associated with an increase of the

tidal amplitude. This finding appears in line with what was concluded in other powerful estuarine systems adjacent broad, shallow shelves (Pickering et al., 2017; Tazkia et al., 2017; van Maanen and Sottolichio, 2018; Schindelegger et al., 2017; Khan et al., 2020). The origin of the higher sea level in the Cabo Norte region when the Amazon runoff is accounted for (in REF) compared to the case when it is not (in NoAMZ), can be either steric (linked to the lighter density of the plume waters) or manometric (linked to the mass effect of the riverine water bulge) (Durand et al., 2019; Gregory et al., 2019). The two barotropic experiments, carried out with and without the Amazon runoff forcing, show a mean sea level roughly identical in the region of Cabo Norte (within 1 cm; not shown). This implies that the difference in mean sea level between the two stratified experiments (with vs. without the Amazon forcing) is essentially driven by steric effects. The very strong sensitivity of the tide to the regional sea level suggested by our model over the region of Cabo Norte is probably linked to the specific geometry of this embayment, favouring the resonance of semi-diurnal tidal constituents (Beardsley et al., 1995). The last effect through which tide can be altered in river plume regions is through the inhibition of the bottom friction by the vertical density gradient underlying the river plume (e.g. Kang et al. 2002). The lower M2 amplitude observed in our barotropic experiment (BRTP) compared to REF experiment suggests that this mechanism contributes to the higher M2 amplitude in REF, typically by half a dozen cm.

The seasonal variability of the tidal characteristics exhibited by our model around Cabo Norte, with minimum amplitude in boreal spring and maximum amplitude in fall, does not appear to be driven by the seasonal variability of the Amazon discharge. Indeed, both the reference simulation and the Amazon-free NoAMZ sensitivity experiment show a similar seasonal evolution. This echoes to the finding of Molinas et al. (2014), who concluded that the variability of the position of the salinity front located at the forehead of the Amazon freshwater plume on the continental shelf is primarily driven by the variability of the tide and of the wind, much more than by the variability of the river discharge. However the Amazon plume is known to present a marked seasonal variability of the vertical density stratification at the basis of the Amazon fresh plume, driven by the seasonal cycle of the runoff (Geyer and Kineke, 1995). Our model suggests that the seasonal variability of the tidal amplitude over the Amazonian shelf is not driven by the seasonal variability of the plume stratification, as this seasonal evolution of the tide remains alike in the vertically-stratified and in the barotropic model

experiments. This stands in contrast with what was found in previous studies dealing with other tropical shelves receiving massive, seasonally-varying freshwater discharges such as the East China Sea (Kang et al., 2002). The characteristics of the tide over the Amazonian shelf, as in any coastal region, integrate a variety of factors acting over a broad range of spatial scales, from local to regional (Haigh et al., 2019). The seasonal variability of the tidal characteristics around Cabo Norte reflects the seasonal variability of the sea level in the outer shelf region, much more than the seasonal variability of the local sea level. Similarly with the time-mean effect of the Amazon discharge, this relationship is suggestive of a mechanism of seasonal modulation of the bottom friction by the seasonal modulation of the water column thickness further offshore, the season of highest sea level corresponding to the season of highest tidal amplitude. The seasonal evolution of the offshore sea level is known to result from direct equatorial wind forcing and contributions of waves generated by boundary reflection (Ding et al. 2009).

6. Concluding remarks

This study investigates the impact of the Amazon outflow on the tidal characteristics over the adjacent continental shelf. The embayment located immediately to the North of Cabo Norte, corresponding to the regional maximum of tidal range, appears as the main zone of tidal impact of the Amazon discharge. There, we could conclude to an overall increase of the tidal range by more than twenty cm, partly driven by the reduced bottom friction effect of the steric sea level bulge associated with the Amazon plume, and partly driven by the reduced bottom friction effect associated with the density stratification at the bottom of the plume. This region is bordered by a low-lying, flat coastal floodplain (Nittrouer et al., 2021; Fassoni-Andrade et al., 2021), and exhibits a particularly energetic morphodynamics (Gensac et al., 2016; Santos et al., 2018). Over the region, the impact of extreme water levels on the riparian societies and ecosystems is well identified (Szabo et al., 2016; Mansur et al., 2016). In a social and ecological context where every centimeter of water level counts, and keeping in mind the dominance of the tide on the overall variability of the water level there, our study calls for a careful consideration of the Amazon outflow in the next generation of tidal models of the Northern coast of South America.

There are several limitations in the present study. Our model has a limited horizontal resolution, it relies on a basic representation of the near-shore bathymetry, it excludes the inner Amazon estuary, and we did not attempt any regional tuning of the bottom friction. These limitations are probably largely responsible for the limited skills of the modeled tide in the immediate vicinity of the mouths of the Amazon. A dedicated revisit of the present study with a high-resolution hydrodynamic model explicitly comprising the lower Amazon estuary, and regionally calibrated in terms of bottom roughness, is certainly timely.

As a matter of fact, the sea level rise induced by the Amazon outflow around Cabo Norte, analyzed in the present study, amounting to ten centimeters, is of comparable magnitude to the global sea level rise observed along the 20th century (Church and White 2011). In the context of the ongoing 21st century global sea level rise, and keeping in mind that the rise expected by the end of this century is much larger than what occurred during the past century (Oppenheimer et al., 2019), our study calls for a revisit of the processes we identified, in conditions when the mean sea level will largely exceed the level of today.

Acknowledgements

FD and ACFA were supported by supported by Horizon 2020 (EOSC-synergy, grant no. 857647). We are thankful to Marinha do Brasil, the Brazilian Navy, for the provision of the tide gauge records. Valdenira Ferreira dos Santos (IEPA, Macapá, Brazil) provided the Ponta Guará tide gauge data. Valentin Ruault provided Figure 1. Jamal Uddin Khan shared insights on the harmonic analysis of the data. Supercomputing facilities were provided by GENCI project GEN7298. Jérôme Chanut and Rachid Benshila helped with the embedded numerical modeling setup.

References

Allain, D.J., 2016. TUGOm Tidal Toolbox (ftp://ftp.legos.obs-mip.fr/pub/ecola/tools/ttb.pdf).

Andersen, O. B., Woodworth, P. L., Flather, R. A., 1995. Intercomparison of recent ocean

tide models. Journal of Geophysical Research 100(C12),282–282. doi: 10.1029/95JC02642

Beardsley, R. C., Candela, J., Limeburner, R., Geyer, W. R., Lentz, S. J., Castro, B. M., et al., 1995. The M2 tide on the Amazon Shelf. Journal of Geophysical Research 100(C2), 2283–2319. https://doi.org/10.1029/94JC01688

Blayo, E., Debreu, L., 1999. Adaptive mesh refinement for finite‐difference ocean models: First experiments. Journal of Physical Oceanography 32, 1239–1250.

Carrère, L., Lyard, F., Cancet, M., Guillot, A., Roblou, L., 2012. FES2012: A new global tidal model taking advantage of nearly 20 years of altimetry. Paper presented at the Symposium 20 Years of Progress in Radar Altimetry, Venice, Italy.

Carrère, L., Lyard, F., Cancet, M., Guillot, A., Picot, N., 2016. Finite Element Solution FES2014, a new tidal model – Validation results and perspectives for improvements, in ESA Living Planet Conference, Prague.

Church, J. A., White, N.J., 2011. Sea-level rise from the late 19th to the early 21st century. Surv. Geophys. 32, 585–602.

Ding, H., Keenlyside, N. S., Latif, M., 2009. Seasonal cycle in the upper equatorial Atlantic Ocean. J. Geophys. Res. 114, C09016. doi:10.1029/2009JC005418

Durand, F., Piecuch, C.G., Becker, M., Papa, F., Raju, S.V., Khan, J.U., Ponte, R.M., 2019. Impact of Continental Freshwater Runoff on Coastal Sea Level. Surv. Geophys. 40. 1437–1466. doi.org/10.1007/s10712-019-09536-w.

Dussin, R., Barnier, B., Brodeau, L., 2016. Updated description of the DFS5 forcing data set: The making of Drakkar forcing set DFS5, DRAKKAR/MyOcean Rep. 01‐04‐16, Lab. of Glaciol. and Environ. Geophys., Grenoble, France.

Fassoni-Andrade, A. C., Durand, F., Moreira, D., Azevedo, A., dos Santos, V. F., Funi, C., Laraque, A., 2021. Comprehensive bathymetry and intertidal topography of the Amazon estuary, Earth Syst. Sci. Data Discuss. https://doi.org/10.5194/essd-13-2275-2021.

Fontes, R. F. C., Castro, B. M., Beardsley, R. C., 2008. Numerical study of circulation on the inner Amazon Shelf. Ocean Dynamics 58(3‐4), 187–198. https://doi.org/10.1007/s10236‐008‐0139‐4.

Gabioux, M., Vinzon, S. B., Paiva, A. M., 2005. Tidal propagation over fluid mud layers on the Amazon shelf. Cont Shelf Res 25, 113–125.

Gallo, M. N., Vinzon, S. B., 2005. Generation of overtides and compound tides in Amazon estuary. Ocean Dyn. 55(5–6), 441–448. doi:10.1007/s10236-005-0003-8.

Gensac, E., Martinez, J. M., Vantrepotte, V., Anthony, E. J., 2016. Seasonal and inter-annual dynamics of suspended sediment at the mouth of the Amazon river: The role of continental and oceanic forcing, and implications for coastal geomorphology and mud bank formation. Continental Shelf Research 18, 49-62. https://doi.org/10.1016/j.csr.2016.02.009

Gévaudan, M., Jouanno, J., Durand, F., Morvan, G., Renault, L., Samson, G., 2021. Influence of ocean salinity stratification on the tropical Atlantic Ocean surface. Climate Dynamics. doi: 10.1007/s00382-021-05713-z.

Geyer, W., Kineke, G., 1995. Observations of currents and water properties in the Amazon Frontal Zone. Journal of Geophysical Research 100.,2321-2339.

Giffard, P., Llovel, W., Jouanno, J., Morvan, G., Decharme, B., 2019. Contribution of the Amazon River Discharge to Regional Sea Level in the Tropical Atlantic Ocean. Water 11(11), 2348. https://doi.org/10.3390/w11112348.

Gregory, J.M., Griffies, S.M., Hughes, C.W. *et al.*, 2019. Concepts and Terminology for Sea Level: Mean, Variability and Change, Both Local and Global. Surv. Geophys. 40, 1251–1289. https://doi.org/10.1007/s10712-019-09525-z.

Haigh, I.D., Pickering, M.D., Green, J.A.M., Arbic, B.K., Arns, A., Dangendorf, S., Hill, D., et al., 2019. The tides they are A-changin': a comprehensive review of past and future non-astronomical changes in tides, their driving mechanisms and future implications. Rev. Geophys. https://doi.org/10.1029/2018RG000636.

Hernandez, O., Jouanno, J., Durand, F., 2016. Do the Amazon and Orinoco freshwater plumes really matter for hurricane-induced ocean surface cooling? J. Geophys. Res. Ocean 121, 2119–2141. doi:10.1002/2015JC011021.

HYBAM (2018). Contrôles géodynamique, hydrologique et biogéochimique de l'érosion/altération et des transferts de matière dans les bassins de l'Amazone, de l'Orénoque et du Congo. Available at http://www.ore‐hybam.org.

Kang, S. K., Foreman, M. G .G. et al., 2002. Two-layer tidal modeling of the Yellow and East China Seas with application to seasonal variability of the M2 tide. J. Geophys. Res. 107(C3). doi:10.1029/2001JC000838.

525 Khan, J. U., Ansary, N., Durand, F., Testut, L., Ishaque, M., Calmant, S., Krien, Y., Islam, A. K.
526 S. M., Papa, F., 2019. High Resolution Intertidal Topography from Sentinel-2 Multi-
527 Spectral Imagery: Synergy between Remote Sensing and Numerical Modelling.
528 Remote Sensing 11, 2888. doi:10.3390/rs11242888.
529 Khan, J. U., Durand, F., Testut, L., Krien, Y., Islam, A. K. M. S., 2020. Sea level rise inducing
530 tidal modulation along the coasts of Bengal delta. Continental Shelf Research 211.
531 https://doi.org/10.1016/j.csr.2020.104289.
532 Kosuth, P., Callede, J., Laraque, A., Filizola, N., Guyot, J. L., Seyler, P., Fritsch, J. M.,
533 Guimarães, V., 2009. Sea-tide effects on flows in the lower reaches of the Amazon
534 River. Hydrol. Process. 23, 3141–3150. doi:10.1002/hyp.7387.
535 Krien, Y., Mayet, C., Testut, L., Durand, F., Tazkia, A. R., Islam, A. K. M. S., Gopalakrishna,
536 V.V., et al., 2016. Improved bathymetric dataset and tidal model for the northern
537 Bay of Bengal. Mar. Geodes. 39 (6), 422–438. https://doi.org/10.1080/
538 01490419.2016.1227405.
539 Latrubesse, E., Arima, E., Dunne, T. *et al.,* 2017. Damming the rivers of the Amazon basin.
540 Nature 546, 363–369. https://doi.org/10.1038/nature22333.
541 Le Bars, Y., Lyard, F., Jeandel, C., Dardengo, L., 2010. The AMANDES tidal model for the
542 Amazon estuary and shelf. Ocean Modelling 31(3–4), 132–149.
543 https://doi.org/10.1016/j.ocemod.2009.11.001
544 Lentz, S. J., & Limeburner, R. (1995). The Amazon River plume during AMASSEDS:
545 Spatial characteristics and salinity variability. Journal of Geophysical Research,
546 100(C2), 2355. https://doi.org/10.1029/94jc01411.
547 Locarnini, R. A., A. V. Mishonov, J. I. Antonov, T.P. Boyer, H. E. Garcia, O. K. Baranova, M.
548 M.Zweng, C. R. Paver, J. R. Reagan, D. R. Johnson, M. Hamilton, D. Seidov, 2013.
549 World Ocean Atlas 2013. Vol. 1: Temperature. S. Levitus, Ed.; A.Mishonov,
550 Technical Ed. NOAA Atlas NESDIS73, 40 pp
551 Molinas, E., Vinzon, S. B., de Paula Xavier Vilela, C., Gallo, M. N., 2014. Structure and
552 position of the bottom salinity front in the Amazon Estuary. Ocean Dyn. 64(11),
553 1583–1599. doi:10.1007/s10236-014-0763-0.
554 Molinas, E., Castro Carneiro, J., Vinzon, S., 2020. Internal tides as a major process in
555 Amazon continental shelf fine sediment transport. Marine Geology 430. doi
556 10.1016/j.margeo.2020.106360.

Madec, G., 2014. “NEMO ocean engine” (Draft edition r5171), Note du Pôle de modélisation 27, Inst. Pierre‐Simon Laplace, France, ISSN No 1288‐1619.

Mansur, A. V., Brondízio, E. S., Roy, S., Hetrick, S., Vogt, N. D., Newton, A., 2016. An assessment of urban vulnerability in the Amazon Delta and Estuary: a multi-criterion index of flood exposure, socio-economic conditions and infrastructure, Sustain. Sci. 11(4), 625–643. doi:10.1007/s11625-016-0355-7.

Müller, M., Cherniawsky, J.Y., Foreman, M.G.G., *et al.*, 2014. Seasonal variation of the M_2 tide. Ocean Dynamics 64, 159–177. https://doi.org/10.1007/s10236-013-0679-0

Nikiema, O., Devenon, J.-L., Baklouti, M., 2007. Numerical modeling of the Amazon River plume. Continental Shelf Research 27(7), 873–899.

Nittrouer, C., DeMaster, D., Kuehl, S., Figueiredo, A., Sternberg, R., Faria, L. E. C., Silveira, O., Allison, M., Kineke, G., Ogston, A., Souza Filho, P., Asp, N., Nowacki, D., Fricke, A., 2021. Amazon Sediment Transport and Accumulation Along the Continuum of Mixed Fluvial and Marine Processes. Ann. Rev. Mar. Sci. 13(1), 1–36. doi:10.1146/annurev-marine-010816-060457.

Oppenheimer, M., Glavovic, B., Hinkel, J., van de Wal, R., Magnan, A.K., Abd- Elgawad, A., Cai, R., et al., 2019. Sea level rise and implications for low lying islands, coasts and communities. In: IPCC Special Report on the Ocean and Cryosphere in a Changing Climate.

Pickering, M. D., Horsburgh, K. J., Blundell, J. R., Hirschi, J. J. M., Nicholls, R. J., Verlaan, M., Wells, N. C., 2017. The impact of future sea‐level rise on the global tides, Continental Shelf Research 142, 50–68. doi:10.1016/j.csr.2017.02.004.

Pugh, D. T., Woodworth, P. L., 2014. Sea-Level Science: Understanding Tides, Surges, Tsunamis and Mean Sea-Level Changes. Cambridge: Cambridge Univ. Press., 408pp.

Reffray G., Bourdalle-Badie, R., Calone, C., 2015. Modelling turbulent vertical mixing sensitivity using a 1-D version of NEMO. Geosci. Model Dev. 8, 69–86. doi:10.5194/gmd-8-69-2015.

Ruault, V., Jouanno, J., Durand, F., Chanut, J., Benshila, R., 2020. Role of the Tide on the Structure of the Amazon Plume: A Numerical Modeling Approach, J. Geophys. Res. Ocean. 125(2), 1–17. doi:10.1029/2019jc015495.

588 Santos, E. S., Pinheiro Lopes, P. P., da Silva Pereira, H. H., de Oliveira Nascimento, O.,
589 Rennie, C. D., O'Reilly Sternberg, L. S. L., da Cunha, A. C., 2018. The impact of
590 channel capture on estuarine hydro-morphodynamics and water quality in the
591 Amazon delta, Science of The Total Environment 624, 887-899. doi
592 10.1016/j.scitotenv.2017.12.211.
593 Schindelegger, M., Green, J. A. M., Wilmes, S. B., Haigh, I. D., 2018. Can we model the effect
594 of observed sea level rise on tides? Journal of Geophysical Research Oceans 123,
595 4593-4609. doi:10.1029/2018JC013959.
596 Szabo, S., Brondizio, E.S., Hetrick, S., Matthews, Z., Renaud, F., Sebesvari, Z., et al., 2016.
597 Population dynamics, delta vulnerability and environmental change: comparison
598 of the Mekong, Ganges–Brahmaputra and Amazon delta regions. Sustain Sci.
599 doi: 10.1007/s11625-016-0372-6
600 Talke, S. A., Jay, D.A., 2020. Changing tides: the role of natural and anthropogenic factors.
601 Annual Review of Marine Science 12 (1), 121–151. https://doi.org/
602 10.1146/annurev-marine-010419-010727.
603 Tazkia, A. R., Krien, Y., Durand, F., Testut, L., Islam, A. K. M. S., Papa, F., Bertin, X., 2017.
604 Seasonal modulation of M2 tide in the northern Bay of Bengal. Continent. Shelf Res.
605 137, 154–162. https://doi.org/10.1016/j.csr.2016.12.008.
606 Umlauf, L., Burchard, H., 2003. A generic length-scale equation for geophysical
607 turbulence models. Journal of Marine Research 61 (31), 235–265.
608 van Maanen, B., Sottolichio, A., 2018. Hydro- and sediment dynamics in the Gironde
609 estuary (France): Sensitivity to seasonal variations in river inflow and sea level
610 rise. Continental Shelf Research 165, 37-50. doi 10.1016/j.csr.2018.06.001.
611 Weatherall, P., Marks, K. M., Jakobsson, M., Schmitt, T., Tani, S., Arndt, J. E., Rovere, M.,
612 Chayes, D., Ferrini, V., and Wigley, R., 2015. A new digital bathymetric model of the
613 world's oceans, Earth Sp. Sci. 2, 331–345.
614 https://doi.org/10.1002/2015EA000107.
615 Zweng, M. M., J. R. Reagan, J. I. Antonov, R. A.Locarnini, A. V. Mishonov, T. P. Boyer,
616 H. E.Garcia, O. K. Baranova, D. R. Johnson, D. Seidov, and M. M. Biddle, 2013. World
617 Ocean Atlas 2013.Vol. 2: Salinity. S. Levitus, Ed., A. Mishonov,Technical Ed.
618 NOAA Atlas NESDIS 74, 39 pp.
619

Model simulation name	Tidal forcing	Wind forcing	Amazon discharge forcing	Density stratification	Period of the simulation
REF	✓	✓	✓	✓	2014-2015
NOAMZ	✓	✓		✓	2014-2015
BRTP	✓	✓	✓		2015
BRTPnoAMZ	✓	✓			2015

Table 1. Characteristics of the modeling experiments

Station (record length)	Observation			Model		
		Ao (cm)	ϕo (degrees)	Am (cm)	ϕm (degrees)	Error (cm)
Cabo Maguari (48.41662°W,0.25298°S) (1 month)	M2	131	0°	164	-17°	54
	S2	38	18°	56	13°	18
	σ					**40**
Camarão Tuba (49.51987°W,0.23006°S) (1 month)	M2	152	75°	89	82°	65
	S2	41	80°	26	99°	18
	σ					**48**
Chaves (49.98383°W,0.1664°S) (1 month)	M2	117	94°	94	144°	92
	S2	21	137°	22	159°	8
	σ					**65**
Ponta do Céu (50.11686°W,0.76510°N) (1 year)	M2	174	91°	172	94°	9
	S2	36	123°	43	126°	7
	σ					**8**
Ponta Guará (49.88333°W,1.21667°N) (1 month)	M2	153	43°	143	40°	12
	S2	40	62°	35	69°	6
	σ					**9**

Table 2. Comparison between the observed and model tidal constituents at the five in situ stations displayed in Figure 1b. The error is defined as the modulus of the complex difference. σ denotes the complex error.

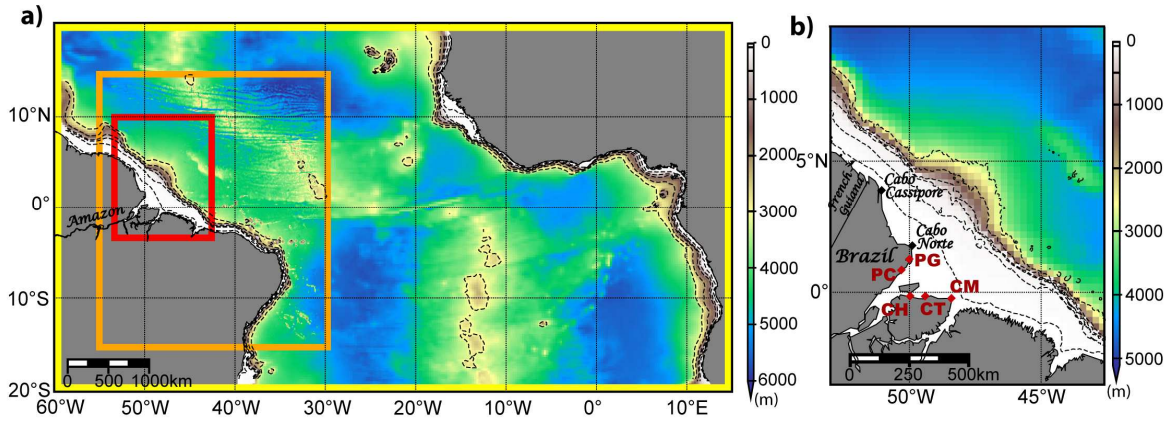

Fig. 1. Study region with model bathymetry. Yellow = coarse model grid (1/4°); Orange = intermediate grid (1/12°); Red = fine grid (1/36°). In (b), zoom on the domain of the fine grid, with the locations of the five tide gauge stations (CM = Cabo Maguari; CT = Camarão Tuba; CH = Chaves; PC = Ponta do Céu; PG = Ponta Guará). The 15m, 80m, 500m, 1000m, 2000m and 3000m isobaths are shown in dashes.

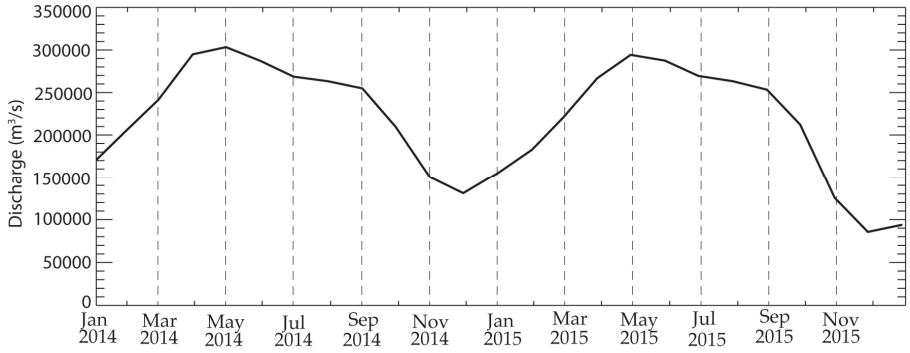

637
638
639 **Fig. 2.** Evolution of the Amazon discharge from HYBAM (2018) in Óbidos station used to force
640 the model (in m^3/s).
641

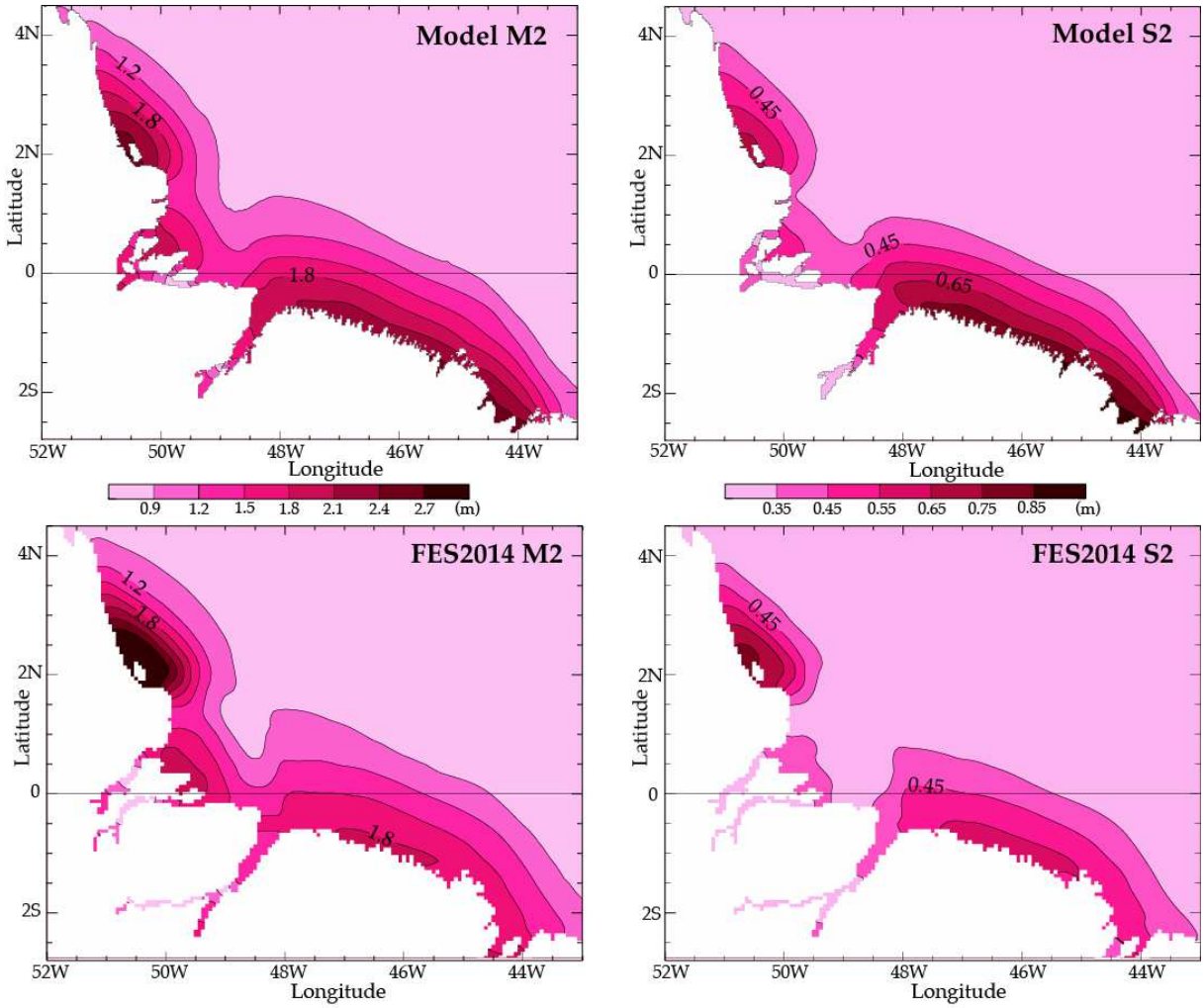

Fig. 3. Tidal amplitudes from the model (REF experiment) and FES2014 tidal atlas, for M2 and S2 tidal constituents (in m).

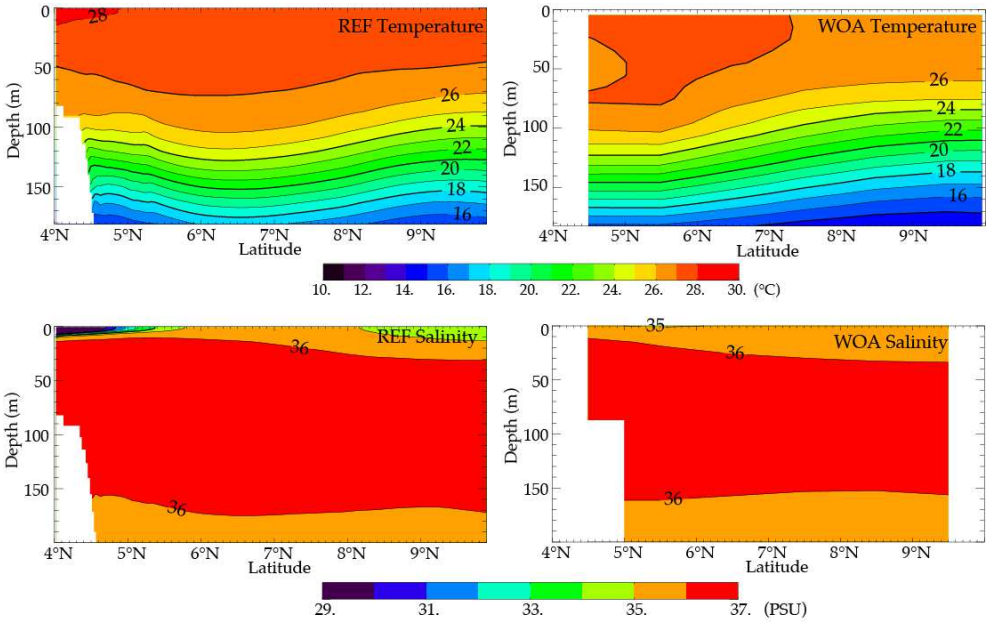

Fig. 4. Meridional sections of climatological modelled (from REF simulation, left column) and observed (from World Ocean Atlas, right column) temperature and salinity in the upper 200 m along 50°W, off the Amazon mouth.

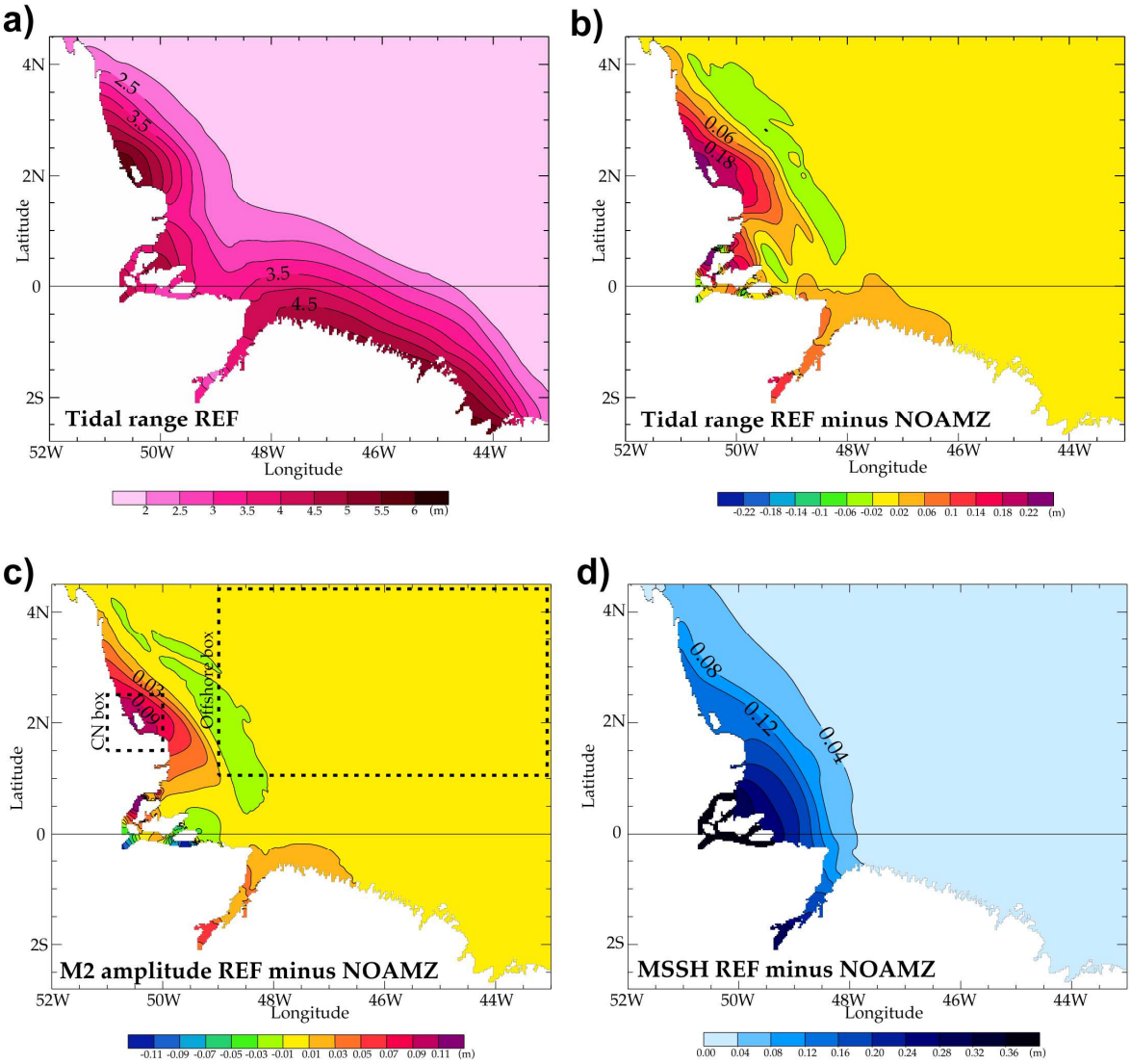

Fig. 5. (a) Mean tidal range in the model (REF experiment). (b) Difference of mean tidal range between REF and NoAMZ experiments. (c) Difference of amplitude of M2 tide between REF and NoAMZ experiments. (d) Difference of mean sea surface height between REF and NoAMZ experiments (in m). Figure (c) shows the limits of boxes around Cabo Norte ("CN box") (50°W-51°W;1.5°N-2.5°N) and offshore ("Offshore Box") (43°W-49°W;1°N-4.5°N) used for subsequent analyses.

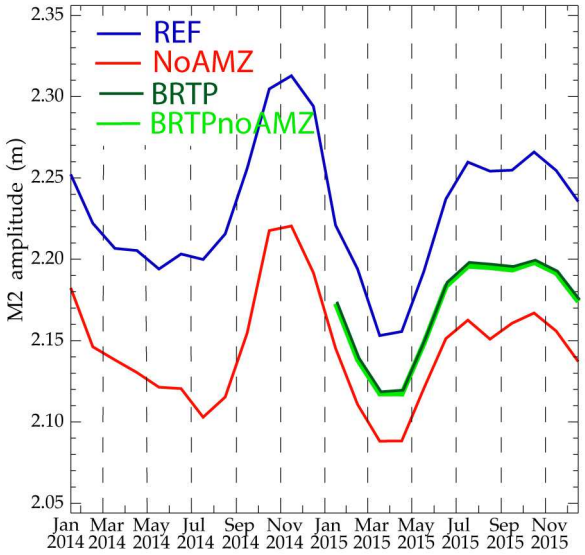

Fig. 6. Monthly evolution of M2 tide amplitude of the various model experiments, averaged over the box "Cabo Norte"

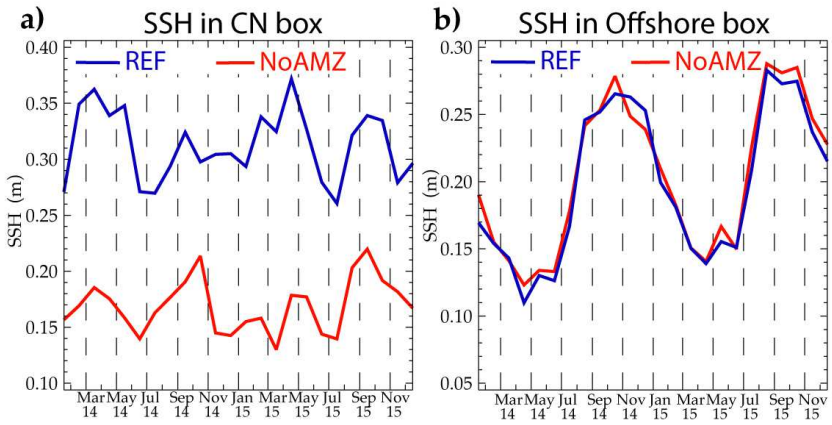

Fig. 7. (a) Monthly evolution of the sea surface height over the box "Cabo Norte", for the REF experiment (blue) and for the NoAMZ experiment (red). (b) same as (a), over the box "Offshore".